

## Long-Term Variation of Dust Devils in East Asia During 1959–2021

P. Du<sup>1</sup>, Z. Huang<sup>1,2</sup> , S. Tang<sup>1</sup>, Q. Dong<sup>1</sup>, J. Bi<sup>1</sup>, X. Yu<sup>1</sup>, and Q. Gu<sup>1</sup>

<sup>1</sup>Collaborative Innovation Center for Western Ecological Safety, College of Atmospheric Sciences, Lanzhou University, Lanzhou, China, <sup>2</sup>Collaborative Innovation Center for Western Ecological Safety, Lanzhou University, Lanzhou, China

### Key Points:

- An overall downward trend in potential dust devil and dusty plume (PDDP) frequency was found in East Asia during 1959–2021
- PDDP occurrence in the Taklimakan Desert decreased during 1959–2021 while they increased significantly in the Gobi Desert
- There is a negative correlation between precipitation and PDDP frequency

### Supporting Information:

Supporting Information may be found in the online version of this article.

### Correspondence to:

Z. Huang,  
[huangzhongwei@lzu.edu.cn](mailto:huangzhongwei@lzu.edu.cn)

### Citation:

Du, P., Huang, Z., Tang, S., Dong, Q., Bi, J., Yu, X., & Gu, Q. (2023). Long-term variation of dust devils in East Asia during 1959–2021. *Journal of Geophysical Research: Atmospheres*, 128, e2022JD038013. <https://doi.org/10.1029/2022JD038013>

Received 13 OCT 2022

Accepted 29 MAR 2023

### Author Contributions:

**Conceptualization:** Z. Huang  
**Formal analysis:** P. Du, Z. Huang  
**Investigation:** P. Du, Z. Huang  
**Methodology:** P. Du, Z. Huang  
**Software:** P. Du  
**Supervision:** Z. Huang  
**Writing – original draft:** P. Du  
**Writing – review & editing:** Z. Huang

**Abstract** Dust devils play an important role in dust transport by carrying it from the surface into the atmosphere, especially in summer. However, information on how dust devils changed in the past decades and what caused these changes remains lacking. Based on thermodynamic criteria and ERA5 reanalysis data set, this study investigated the long-term variation of favorable conditions for dust devil occurrence in East Asia over the past 63 years and defined it as potential dust devil and dusty plume (PDDP) occurrence in hours. Annual mean frequency of PDDP in East Asia was approximately 217.2 hr from 1959 to 2021. An overall downward trend in PDDP frequency has been found over 63 years in East Asia among which strong PDDPs drop significantly at the fastest rate while the weak ones dropped insignificantly. Moreover, PDDP frequency in the Gobi Desert increased but they decreased in the Taklimakan Desert. The monthly variation of PDDP shows a single-peak structure with a tendency for the peak to move from June to July. For the diurnal changes, PDDP mainly occurred between 10:00 and 16:00 at local time (LT), with over 60% of them happening between 12:00 LT and 14:00 LT. We also found a negative correlation between precipitation and PDDP occurrence. This study provides a comprehensive understanding of favorable conditions for dust devil occurrence in East Asia over the past decades, which is of great importance to further evaluate its impact on climate, environment as well as ecosystem.

**Plain Language Summary** Dust devils are convective vertical vortices, commonly found during summer in arid and semi-arid regions. Since dust storms usually occur in spring and winter but rarely in summer, dust devils become a major means of transporting dust aerosols into the atmosphere in summer which could have further impacts on weather and climate with aerosol–radiation and aerosol–cloud interactions. In addition, the dust that has been lifted in the atmosphere could function as a carrier of bioaerosols which are efficient ice nuclei and cause adverse health effects. Therefore, dust devils have great research significance. In this study, we investigated the long-term trend of favorable conditions for dust devil occurrence and defined it as potential dust devil and dusty plume (PDDP). We have found an overall downward trend of PDDP occurrence in East Asia during 1959–2021 where the strong ones dropped significantly at the fastest rate. For small regions, PDDP in the Taklimakan Desert decreased during 1959–2021 while they increased significantly in the Gobi Desert. There is also a negative correlation between precipitation and PDDP frequency.

## 1. Introduction

Dust devils are convective vertical vortices caused by uneven surface heating, commonly happening in arid and semi-arid regions (Klose et al., 2016). The occurrence of dust devils requires certain meteorological conditions such as local vorticity and strong frequent solar insolation which can lead to atmospheric vertical instability with super adiabatic lapse rate (Balme & Greeley, 2006). Flat terrain with dust sources is also a prerequisite for the presence of dust devils. Previous study has found that arid areas are the most susceptible to dust devils (Balme & Greeley, 2006). In the presence of dust devils, earlier measurements have shown that the dust concentration in the atmosphere is three orders of magnitude higher than the background value. A typical dust devil can bring approximately 20 kg of dust into the atmosphere, while a very large one with a radius of over 100 m can carry about 15,000 kg of dust during its life span (Koch & Renno, 2005; Renno et al., 2004).

The mineral dust that has been lifted in the air can, directly and indirectly, affect climate, which can in turn alter radiation balance in the atmosphere and act as cloud condensation nuclei to influence precipitation (Ginoux et al., 2001; Z. Huang et al., 2010; Zhang et al., 2022). Direct effect of dust aerosols on radiation balance (through absorption and scattering) influences the energy balance of the earth system (E-cycle), while the organic matters

carried by dust is associated with the carbon cycle (C-cycle) (Dong et al., 2022; Z. Huang et al., 2022; J. Liu et al., 2022; Shao et al., 2011). Besides, the absorption of solar radiation by dust aerosols can also change the relative humidity and stability of the atmosphere (considered as semi-direct effect) and thus modifies cloud properties, such as cloud lifetime and cloud liquid water content (J. Huang et al., 2014; Z. Huang et al., 2018). It is indicated that the frequency of dust devils will increase as vegetation cover decreases (Oke et al., 2007). In the context of global warming, drylands which feed about 38% of the world's population are more sensitive and vulnerable to the risk of drought area expansion and intensification that may increase the frequency of dust devils (J. Huang et al., 2017). Therefore, it is essential to investigate the spatial and temporal distributions of dust devils, and their inter-annual variability and effects.

Field observations have been conducted to investigate the properties of dust devils in the past decades. These studies revealed that the size and duration of a typical dust devil is about 10 to over 100 m and lasts for about 5–15 min which usually occurs between 10:00 LT and 17:30 LT (Balme & Greeley, 2006; Carroll & Ryan, 1970; Hess & Spillane, 1990; Sinclair, 1973). Dust devil occurrence requires a temperature difference between surface and air of more than 15°C, perhaps more specifically, above 17°C and the favorable wind speeds are about 2–7 m · s<sup>-1</sup> (Ansmann et al., 2009; C. Liu et al., 2016; Oke et al., 2007). Large eddy simulation (LES) has been used as an effective method to study dust devils. Pressure drop is an important indicator of the intensity of dust devils in the LES method because it is related to how fast the vertical winds will be through the pressure-gradient force and it is relatively easy to measure (Gu et al., 2008; Klose & Shao, 2016). Nonetheless, if there is not enough loose material on the surface to be carried into the atmosphere, the loading of dust devil will not increase with more intense pressure drop (Klose et al., 2016; Mason et al., 2014). Based on the LES method, Gu et al. (2010) demonstrated the strong impact of the initial angular momentum of air parcels on the radius of dust devils and significant influence of surface heat flux on updraft velocity. Using a similar method, some studies also showed that particles up to 160 μm in diameter could be rolled into the atmosphere with large ones dropping back to the ground while small ones were lifted to a certain height and transported elsewhere (Gu et al., 2008; Zhao et al., 2004). Recently, there have been some attempts to evaluate the contribution of dust emissions by dust devils. By combining observation data and theory, Koch and Renno (2005) found that the contribution of dust devils to total global dust emissions was up to 35%. By applying thermodynamic criteria, Jemmett-smith et al. (2015) presented the global hourly potential dust devil occurrence, and estimated the amount of dust from dust devils as approximately 3.4% of the global total. Besides, other studies focused on the arid region in northwestern China, mainly around the Taklimakan Desert. Han et al. (2016) estimated that dust devils contributed 53% to the total annual desert dust in western China based on satellite and Lidar observations. Tang et al. (2018) established a new parameterization scheme coupled with WRF-Chem Model and found that dust devils contributed about 30.4 ± 13% to atmospheric dust aerosols in East Asia. By combining observed meteorological data and estimation model, Ma et al. (2020) gave an estimate of 46.5% for the same region. Therefore, there is still large uncertainty about the impacts due to the complexity of dust devils and the lack of knowledge of their characteristics in different regions.

Whilst previous studies presented a general idea of the properties of dust devils and the amount of dust they could bring, they did not dip into the spatial-temporal change and give long-term trends. In addition, East Asia is an important dust source region that contributes about 11% of global dust loading (2.0–3.4 Tg) (Kok et al., 2021). Combined with its geographical location and meteorological conditions, East Asia is a favorable area for dust devils (Jemmett-smith et al., 2015). Nevertheless, there are limited studies that focus on dust devils in East Asia and investigate the effect of different underlying surface types. Until now, information on how dust devil changed in the past decades and what caused these changes is still lacking. Based on thermodynamic criteria and ERA5 reanalysis data set, this study investigated the long-term variation of favorable conditions for dust devil occurrence in East Asia over the past 63 years as potential dust devil and dusty plume (PDDP) occurrence in hours. Section 2 describes the data and methods. The overall distribution and trend of PDDP occurrence in East Asia as well as a detailed discussion of four selected sites with different underlying surface and meteorological conditions are presented in Section 3. Conclusions are given in Section 4.

## 2. Data and Methods

### 2.1. Study Area

Figure 1 presents the four selected regions in East Asia for detailed investigation. We chose the region within the range of 70°–140°E and 15°–55°N for our study. The selection of four regions is based on the annual average

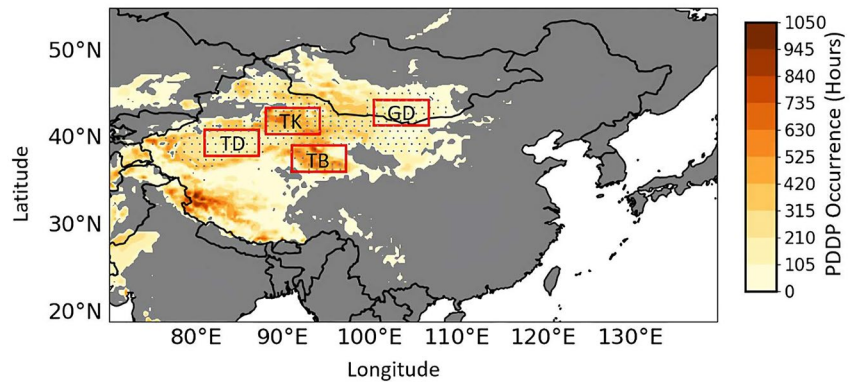


**Figure 1.** Distribution of potential dust devil and dusty plume occurrence during 1959–2021 calculated using ERA5 reanalysis data set. Four study regions are marked by red boxes, gray dots represent typical dust sources in East Asia.

frequency of PDDP and takes dust sources into account. TD, TK, TB, and GD in Figure 1 represent the Taklimakan Desert, Turpan Basin and Kuluketage, Tsaিদam Basin, and Gobi Desert, respectively. The four regions are all located in arid areas with sufficient sand supply. Each region has the same latitude and longitude scale spanning 6.25 longitudes and 3 latitudes (see details in Table 1). Annual mean precipitation was obtained from ERA5 (the fifth generation ECMWF atmospheric reanalysis of the global climate) reanalysis data set, we use the average of 1959–2021 in this study (more details in Section 2.3). Following the Food and Agriculture Organization of the United Nations (FAO), the arid index (AI) is defined as the ratio of the annual precipitation ( $P$ ) to the annual potential evapotranspiration (PET) and calculated by applying the Climate Prediction Center (CPC) monthly datasets at a spatial resolution of  $0.5^\circ$  (Allen et al., 1998; Feng & Fu, 2013; J. Huang et al., 2020). Combined with Feng and Fu (2013), aridity of a region can be classified as dryland ( $P/PET < 0.5$ ), hyper-arid ( $P/PET < 0.05$ ), and arid ( $0.05 < P/PET < 0.2$ ). AI in Table 1 is the average for 2011–2016 and all four regions listed are located in arid region with  $AI < 0.2$  while TB and TK are further in the hyper-arid region. Annual mean PDDP frequency in Table 1 is calculated using the thermodynamic criteria in Section 2.2 and ERA5 reanalysis data set.

## 2.2. Identification of Dust Devils

Basically, the thermodynamic criteria used in the study are from Jemmett-smith et al. (2015) that summarized previous studies and verified them. The criteria include  $w^*/u^* > 5.0$  (Lyons et al., 2008) and  $8.5 \text{ K m}^{-1}$  near-surface lapse rate (Ansmann et al., 2009). High near-surface lapse rate implies strong surface heating due to solar irradiation while  $w^*/u^* > 5.0$  constrains the boundary layer conditions. The  $8.5 \text{ K m}^{-1}$  near-surface lapse rate criterion was derived from observations in North Africa (Ansmann et al., 2009) which is also consistent with that in the Taklimakan Desert (C. Liu et al., 2016). In the  $w^*/u^* > 5.0$  criterion,  $u^*$  and  $w^*$  represent the frictional dissipation and convective buoyancy, respectively. According to Deardorff (1970),  $w^*$  can be calculated using

$$w_* = \left[ \frac{g}{T} h \overline{w'T'} \right]^{1/3} \quad (1)$$

where  $g/\overline{T}$  is the buoyancy parameter for an ideal gas,  $h$  is the height of boundary layer, and  $\overline{w'T'}$  is the kinematic heat flux near the surface that can be obtained by dividing the sensible heat flux by the specific heat of air ( $C_p$ )

**Table 1**  
Basic Information of the Four Regions in This Study

Location	Longitude and latitude range	Underlying surface type	Annual mean precipitation (mm)	Arid Index (AI)	Annual mean dust devil frequency (hours/year)
Taklimakan Desert (TD)	81°E–87.25°E, 38°N–41°N	Desert	39.0 ± 14.2	0.026	203.47 ± 30.26
Turpan Basin and Kuluketage (TK)	88°E–94.25°E, 40.5°N–43.5°N	Bare soil surface	108.8 ± 19.2	0.047	365.10 ± 31.78
Tsaিদam Basin (TB)	91°E–97.25°E, 36.25°N–39.25°N	Bare soil surface	171.3 ± 23.8	0.101	356.14 ± 43.94
Gobi Desert (GD)	100.5°E–106.75°E, 41.5°N–44.5°N	Desert	109.6 ± 25.6	0.076	152.41 ± 21.75

and air density ( $\rho$ ) (Stull, 1988).  $\bar{T}$  is the one-hour boundary layer mean temperature, which can be approximated to 925 hPa potential temperature using Equation 2,

$$\theta = T \left( \frac{P_{00}}{P} \right)^K = T \left( \frac{P_{00}}{P} \right)^{\frac{R}{c_p}} \quad (2)$$

where  $T$  is the surface air temperature,  $P$  is the surface pressure,  $P_{00}$  is the 925 hPa. Near-surface lapse rate ( $\Gamma_{\text{Near-surface}}$ ) in the thermodynamic criteria is calculated using surface and 2 m air temperature that is provided in Equation 3,

$$\Gamma_{\text{Near-surface}} = \frac{(T_{\text{skin}} - T_{2\text{m}})}{2} \quad (3)$$

where  $T_{\text{skin}}$  is skin temperature and  $T_{2\text{m}}$  is 2 m air temperature in ERA5 data set. By applying these thermodynamic criteria, Jemmett-smith et al. (2015) gave the global hourly climatology of PDDP occurrence which is consistent with observations with appropriate daily and seasonal changes. Based on the same criteria, we calculate the occurrence of favorable conditions associated with dust devil and dusty plume (DDP) events in the study area and defined it as PDDP occurrence following the study of Jemmett-smith et al. (2015). The significance of trends in PDDP occurrence was determined using Wald Test with t-distribution of the test statistic in Python, while  $p < 0.01$  ( $p < 0.05$ ) means the null hypothesis (i.e., the fitted slope coefficient is zero) is rejected and the trend is statistically significant at the 99% (95%) confidence level.

### 2.3. ERA5 Reanalysis Data Set

ERA5 is the fifth-generation climate reanalysis data set from ECMWF (the European Centre for Medium-Range Weather Forecasts) that can be assessed by the Copernicus Climate Change Service (Hersbach et al., 2018). Briefly, ERA5 was developed to replace its predecessor ERA-Interim (Dee et al., 2011) with finer spatial grid ( $0.25^\circ \times 0.25^\circ$ ), higher time resolution (hourly), and more vertical levels currently available from 1959 to the present. It was constructed using 12-hourly 4DVar data assimilation model combined with vast amounts of data (e.g., model forecast, data from historical satellite, in-situ observations, etc). The ERA5 outputs used in this paper are hourly grid points of temperature, surface pressure, friction velocity, boundary layer height, surface sensible heat flux, total precipitation, and wind. By using the equations listed above, we can apply the criteria to calculate PDDP frequency.

### 2.4. Uncertainties of Data Set and Method

ERA5 2 m air temperatures have been reported that have discontinuities which are related to the initialization of the analysis windows in the “Known issues” section (<https://confluence.ecmwf.int/display/CKB/ERA5%3A+-data+documentation#ERA5:datadocumentation-Knownissues>) while ERA5-Land 2 m air temperatures don't suffer from non-smooth transitions. However, ERA-Land data set lack variables (i.e., boundary layer height and friction velocity) to calculate the PDDP occurrence. One possible solution is to replace 2 m air temperature in ERA5 with forecast data which can cause a new problem as forecast low-level temperatures suffer from a cold bias over most parts of the globe that is also reported in “Known issues” in the ERA5 document. Therefore, we turn to prove that these discontinuities do not affect the results to a large extent (Figure S1 in Supporting Information S1). Dust devils are very small-scale features, with diameters of  $\sim 100$  m, and last for about 5–15 min. The relatively coarse resolution of ERA5 makes it impossible to give details of potential dust devils and dusty plume occurrence such as the number of DDP occurrence within 1-hr intervals and  $0.25^\circ \times 0.25^\circ$  grid boxes. Instead, we give the frequency of PDDP in hours at grid points. If an hourly condition at a grid point satisfies the thermodynamic criteria, we consider that there is a PDDP occurrence at that hour and record it as 1. Having a very high resolution data set can provide more comprehensive information about dust devils. In addition, as dust devil occurrence normally requires smooth arid terrain and relatively level to gently sloping topography, we select Northwest China Arid Region and Gobi Desert instead of the whole region in East Asia to calculate PDDP occurrence by applying a mask based on the underlying surface type using Google Earth Engine (Balme & Greeley, 2006; Gorelick et al., 2017). By applying this mask, we excluded humid and semi-humid regions with no dust sources as well as Tibetan Plateau (Figure S2 in Supporting Information S1) which is also excluded in the

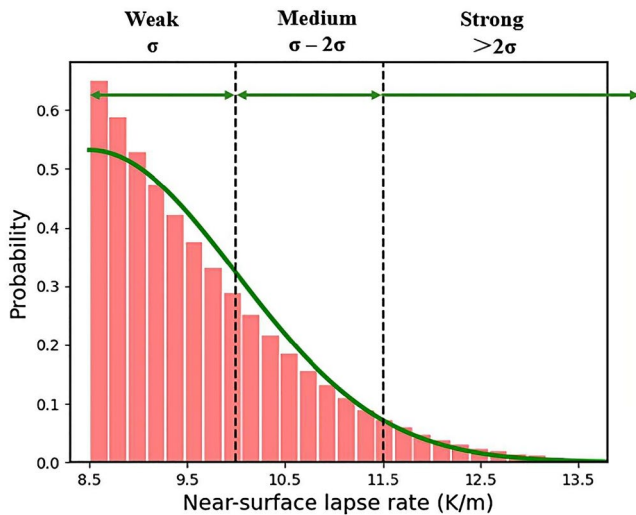


**Figure 2.** Frequency distribution of near-surface lapse rate calculated using ERA5 reanalysis data set.

et al., 2016). In addition, the areas with high frequency of PDDP, that is, the dark-colored areas in Figure 1, largely overlap with the drought-prone areas dotted in gray. This implies that arid and semi-arid regions with dust sources are the areas with frequent occurrence of PDDP, consistent with previous studies (Jemmett-smith et al., 2015; Klose et al., 2016). Within the drought-prone areas dotted in gray, PDDP occurrence tends to increase with the decrease of vegetation cover shown in Figure S5 in Supporting Information S1.

Previous studies have demonstrated that the near-surface lapse rate which represents the development of an unstable lower atmosphere is critical for the occurrence of dust devils. As the lapse rate increases, dust devils tend to become more intense (Oke et al., 2007; Ryan, 1972). Therefore, we use near-surface lapse rate to determine the intensity of PDDP. Near-surface lapse rate for each 1 hr period that shows favorable conditions to dust devil formation from 1959 to 2021 was calculated (see Figure 2). It has a normal distribution with a mean of 8.5 K/m, and a standard deviation of 1.5 K/m. Based on the graph, we give the criteria for classifying different intensities of PDDP. PDDP is considered strong when it is greater than two standard deviations, that is, when the near-surface lapse rate is greater than 11.5°C; medium when it is between one standard deviation and two standard deviations; weak when it is within one standard deviation, that is, the near-surface lapse rate is less than 10°C. All strengths

of PDDP satisfy the criteria of  $w^*/u^* > 5$ . By this definition, the frequency of weak PDDP is approximately 68% of the total frequency of occurrence while the strong ones account for less than 5% of the total frequency. Since the criteria for occurrence of dust devils are given as 8.5 K near-surface lapse rate, we give the horizontal coordinates of Figure 2 starting from 8.5.

### 3. Results and Discussion

#### 3.1. Variation of PDDP in East Asia

According to the thermodynamic criteria (refer to Section 2.2), the calculated annual mean PDDP frequency during 1959–2021 is shown in Figure 1. The shade of color represents PDDP frequency, where the darker the color, the higher PDDP frequency. Arid area is indicated by gray dots. The frequency of annual average PDDP occurring in arid area (dotted in gray) was 217.2 hr which occupy ~2.5% of the yearly time. In contrast, there are few conditions favorable for the occurrence of dust devils in humid areas and at latitudes above 50°N. Most of the places with high frequency of PDDP occurrence have surface solar radiation over 130 W/m<sup>2</sup> (see Figure S4 in Supporting Information S1). For regions at latitudes above 50°N, the reason for few PDDP occurrence is related to insufficient intense surface heating through solar insolation. Therefore, the near-surface atmospheric temperature lapse rate is not strong enough to generate dust devils. For humid regions, rainfall can restrain the occurrence of dust devils by altering soil moisture (Klose et al., 2016; C. Liu

et al., 2016). In addition, the areas with high frequency of PDDP, that is, the dark-colored areas in Figure 1, largely overlap with the drought-prone areas dotted in gray. This implies that arid and semi-arid regions with dust sources are the areas with frequent occurrence of PDDP, consistent with previous studies (Jemmett-smith et al., 2015; Klose et al., 2016). Within the drought-prone areas dotted in gray, PDDP occurrence tends to increase with the decrease of vegetation cover shown in Figure S5 in Supporting Information S1.

According to the criteria discussed earlier, the variation of PDDP of different intensities from 1959 to 2021 based on ERA5 is displayed in Figure 3. The annual mean PDDP frequency from 1959 to 2021 in East Asia was approximately 217.2 hr, of which the frequency of weak PDDP was about 152.8 hr, the frequency of medium ones was roughly 54.4 hr, and the frequency of strong PDDP was about 10.0 hr. The trend of PDDP varied with different intensities. There is a clear downward trend of strong PDDP, while weak dust devil had a great inter-annual fluctuation during 1959–2021, but the trend line of occurrence frequency was basically horizontal in general, and the trend of moderate intensity PDDP was somewhere in between. In Figure 3, all four lines experienced a significant drop in 1992–1993, which could be the effect of the eruption of Mount Pinatubo in June 1991 that caused a global surface cooling of about 0.4°C in the following two years (Self et al., 1993). In East Asia masking area, our results using ERA5

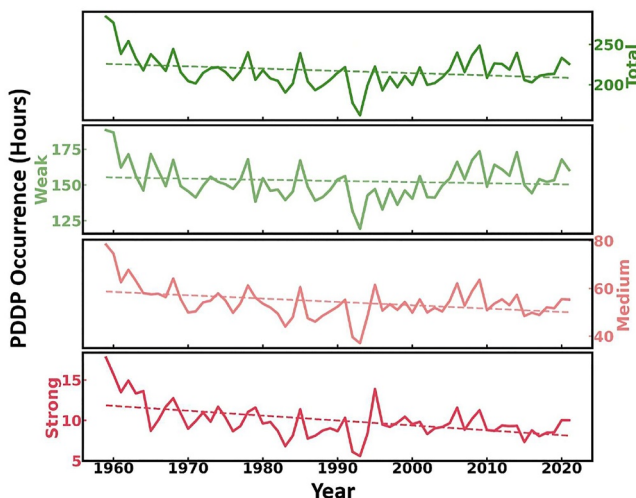


**Figure 3.** Yearly change of potential dust devil and dusty plume for different intensities calculated using ERA5 reanalysis data set.

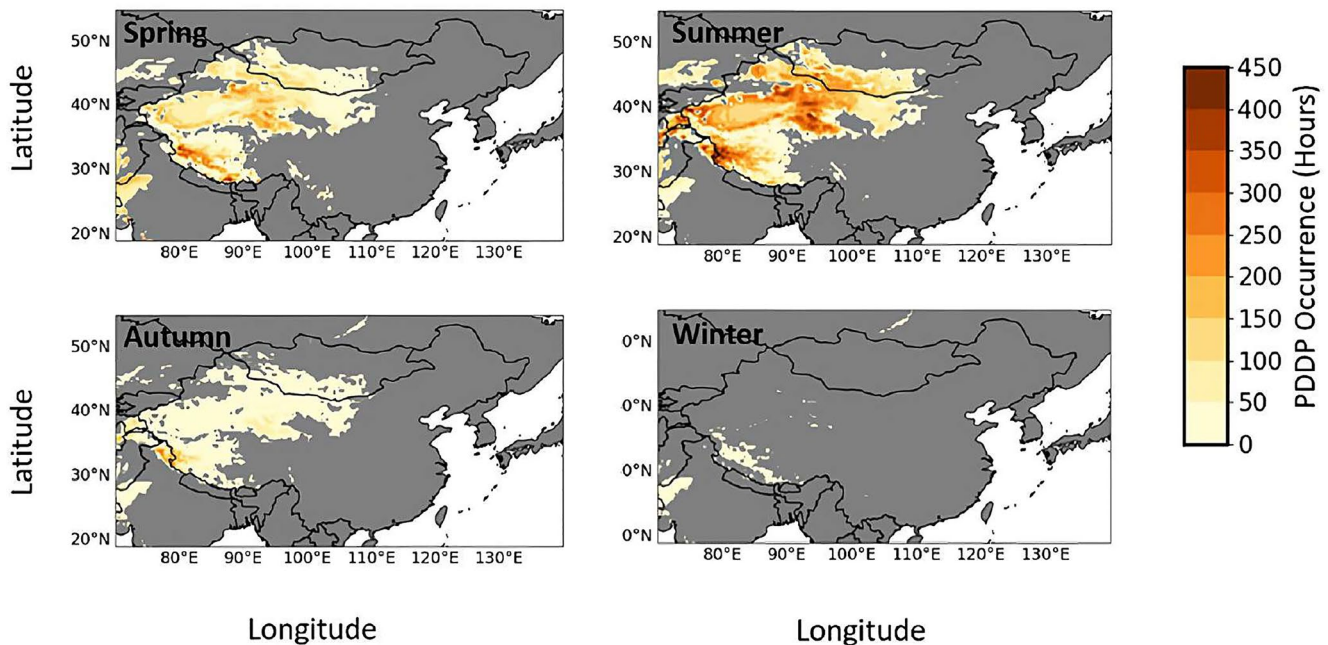


**Figure 4.** Seasonal mean distribution of potential dust devil and dusty plume in East Asia during 1959–2021 calculated using ERA5 reanalysis data set.

showed that annual mean 2 m air temperature during 1992–1993 is 0.5°C lower than the mean temperature for 1959–2021. The decrease in skin temperature was even greater, with the average surface temperature decreasing by 0.7°C in 1992–1993 compared to 1959–2021 and the surface solar radiation in 1992–1993 decreased by 2.8% compared to the average of 1959–2021, from 146.6 to 142.5 W/m<sup>2</sup>. The frequency of PDDP gradually picked up after the eruption with weak PDDP rising to a level of the 1960s. Gillette and Sinclair (1990) using in situ aircraft measurement gave the estimated particle fluxes of dust devils that ranged from  $2 \times 10^{-5}$  kg m<sup>-2</sup> s<sup>-1</sup> for dust devils <3 m in diameter to  $3 \times 10^{-3}$  kg m<sup>-2</sup> s<sup>-1</sup> for dust devils >30 m in diameter while C. Liu et al. (2016) conducted field observation in Taklimakan Desert and estimated the vertical fluxes of near-surface dust emissions between  $5.4 \times 10^{-5}$  and  $9.6 \times 10^{-5}$  kg m<sup>-2</sup> s<sup>-1</sup> with the averages of  $7.1 \times 10^{-5}$  kg m<sup>-2</sup> s<sup>-1</sup>. Although dust flux and the amount of dust brought in each time was small, weak DDP occurred more frequently than strong DDP, and could be regarded as a more significant vehicle for dust to enter the atmosphere from the ground than strong ones.

Figure 4 shows the seasonal mean distribution of PDDP in East Asia during 1959–2021 based on ERA5. Similar to Figure 1, darker color represents higher dust devil frequency. The highest frequency of PDDP occurred in summer which was 139.3 hr, followed by spring (66.1 hr) and autumn (11.7 hr), and almost no PDDP occurred in winter. In summer, the areas with high frequency of PDDP largely coincide with drought areas which have rich sources of dust. Tsaidam Basin and the edge of the Taklimakan Desert showed high value areas for the occurrence of PDDP. Since dust storms usually occurred in spring and winter but rarely in summer, dust devils become a major means of transporting dust aerosols into the atmosphere in summer which could further impact on weather and climate with aerosol–radiation and aerosol–cloud interactions (Gao et al., 2022). In addition, the dust that has been lifted in the atmosphere could function as a carrier of bioaerosols which are efficient ice nuclei and cause adverse health effects, for example, allergies, toxic effects, and infectious diseases (Després et al., 2012). Occurrence of DDP requires frequent strong insolation as well as anomalously high soil temperatures, making it reasonable for them to occur most frequently in summer (Balme & Greeley, 2006). Those results are also consistent with previous studies. Han et al. (2016) indicated that dust devils reached the highest value in summer while Gillette and Sinclair (1990) reported about the seasonality of dust devil with the maximum in summer and the minimum in winter. Based on the LES method, Klose (2014) estimated the number of dust devils and found the largest number of dust devils in spring and summer. More detailed analyses of the monthly and decadal changes are given in the following paragraphs. Wang et al. (2021) found that summer length in the Northern Hemisphere midlatitudes extended from 1951 to 2011 and would continue to lengthen in the 21st century. The extended summer might cause more dust devils which would bring more dust into the atmosphere.

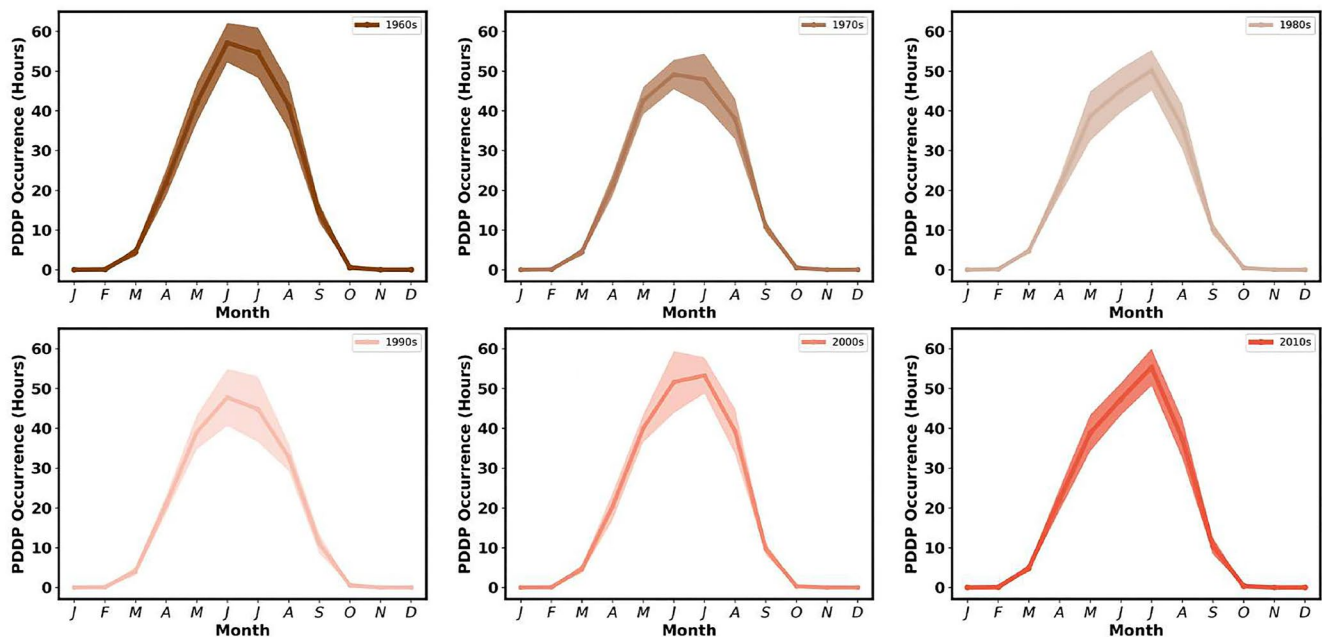


**Figure 5.** Monthly variation of potential dust devil and dusty plume in East Asia over the past decades calculated using ERA5 reanalysis data set.

Besides the distinct seasonal variation, the monthly change in the frequency of PDDP is also evident. Figure 5 shows the monthly variation of PDDP in East Asia for different decades. The thick solid line in the middle is the average occurrence of PDDP for each month of the decade, while the shaded areas next to it are one standard deviation above and one standard deviation below the average, respectively. In these six decades, the annual change in the frequency of PDDP is single-peaked. The frequency of PDDP began to rise from March onwards, reaching a peak in June and July, then gradually declining, and after September the PDDP basically did not occur. The standard deviation of the frequency of PDDP from May to August was large, while the standard deviation of the other months was small, which indicates that the frequency of PDDP varied greatly from May to August during the decade, while the frequency was relatively stable in other months. The large standard deviation from May to August also suggests that for the same region, the effect of different meteorological conditions in different years on the frequency of PDDP is mainly concentrated in May–August, with little effect on PDDP in other months. There is a tendency for the peak to move from June to July (see Figure S3 in Supporting Information S1). PDDP occurrence peaked in June in the 1960s, and it peaked in July in the 2010s with relatively small standard deviation. For the other decades, the maximum value of PDDP frequency fluctuated back and forth between June and July with a large standard deviation. The largest standard deviation occurred in the 1990s, when the effect of the Pinatubo eruption caused greater inter-annual fluctuations in conditions favorable for dust devil occurrence. By comparing the height of the peaks in different subplots, it is found that the frequency of dust devils is high in the 1960s, low in the 1970s, 1980s, 1990s, and then increased in the 2000s and 2010s, which is consistent with the results in Figure 3. Han et al. (2016) gave the similar distribution of dust devil frequency as well as monthly dust emissions by dust devils in his study and found that without the effect of dust storms, the optical thickness monthly variation was consistent with monthly changes in dust devil thermodynamic efficiency which reflects the dust devil strength. Lyons et al. (2008) also found the single peaked distribution of dust devil annual variation in Australia.

### 3.2. Variation of PDDP at Four Specific Regions

Due to the different underlying surface and meteorological conditions in different parts of East Asia, the characteristics of dust devils can vary considerably. Here we describe PDDP occurrence in small areas.

The annual variation of PDDP in four selected regions is shown in Figure 6. TD, TK, TB, and GD represent the Taklimakan Desert, Turpan Basin and Kuluketage, Tsaidam Basin, and Gobi Desert, respectively (see detailed description in Section 2.1). These four regions have different trends in PDDP frequency during 1959–2021, with

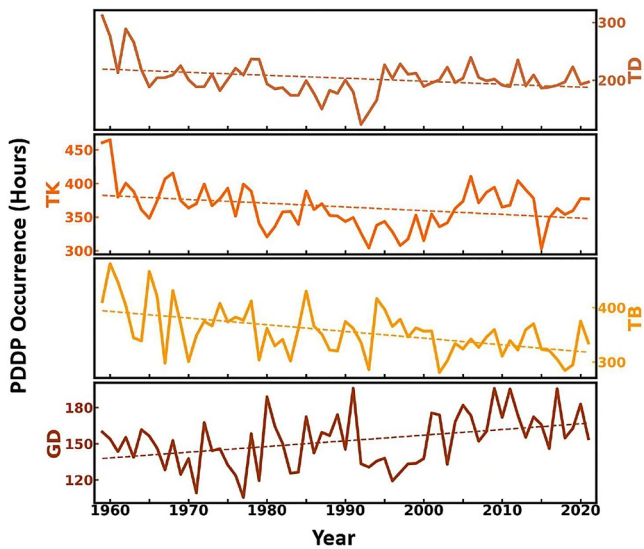


**Figure 6.** Long-term variation of potential dust devil and dusty plume for four sites during 1959–2021.

a decreasing trend for TK, TB, and TD, and an increasing trend for GD. The tendency for TB and GD satisfied  $p < 0.01$ , passing the 0.01 statistical test criterion; while TD and TK passed the 0.05 statistical test criterion. The different tendency indicates the different variability of PDDP frequency in different parts of the same region. Therefore, in future research, in order to have an accurate understanding of dust devil variability, it would be interesting to study not only large scale dust devils, but also small area variability. Annual mean PDDP occurrence for TD, TK, TB, and GD during 1959–2021 were 203.5, 365.1, 356.1, and 152.4 hr, respectively while annual mean surface solar radiation during 1959–2021 for TD, TK, TB, and GD were 154.7, 160.2, 157.5, and 154.1 W/m<sup>2</sup>. The lowest frequency of PDDP in the Gobi Desert is related to lowest annual mean surface solar radiation resulting in lowest near-surface lapse rate. Similar to Figure 3, there was an obvious decline in dust devil frequency during 1992–1993, but the impact of the Pinatubo eruption was distinct for different regions. The eruption of Mount Pinatubo reduced the annual average solar radiation in the TD, TK, TB, and GD regions by 2.5%, 2.4%, 1.0%, and 3.2% in 1992–1993 compared to 1959–2021, respectively, and the annual average 2 m air temperature decreased by 0.57°C, 0.29°C, 0.25°C, and 0.6°C. From the numbers above, it is shown that desert areas are more affected by the eruption of Mount Pinatubo. The different tendencies in the four regions rely on the variation of their local meteorology (details in Section 3.3).

Figure 7 illustrates the monthly changes of PDDP in six decades at the four study regions. To make the tendency more obvious, the vertical coordinates of the four subplots are not unified. Similar to Figure 5, the frequency of PDDP in different locations started to rise in March and reached its maximum in June and July, with almost

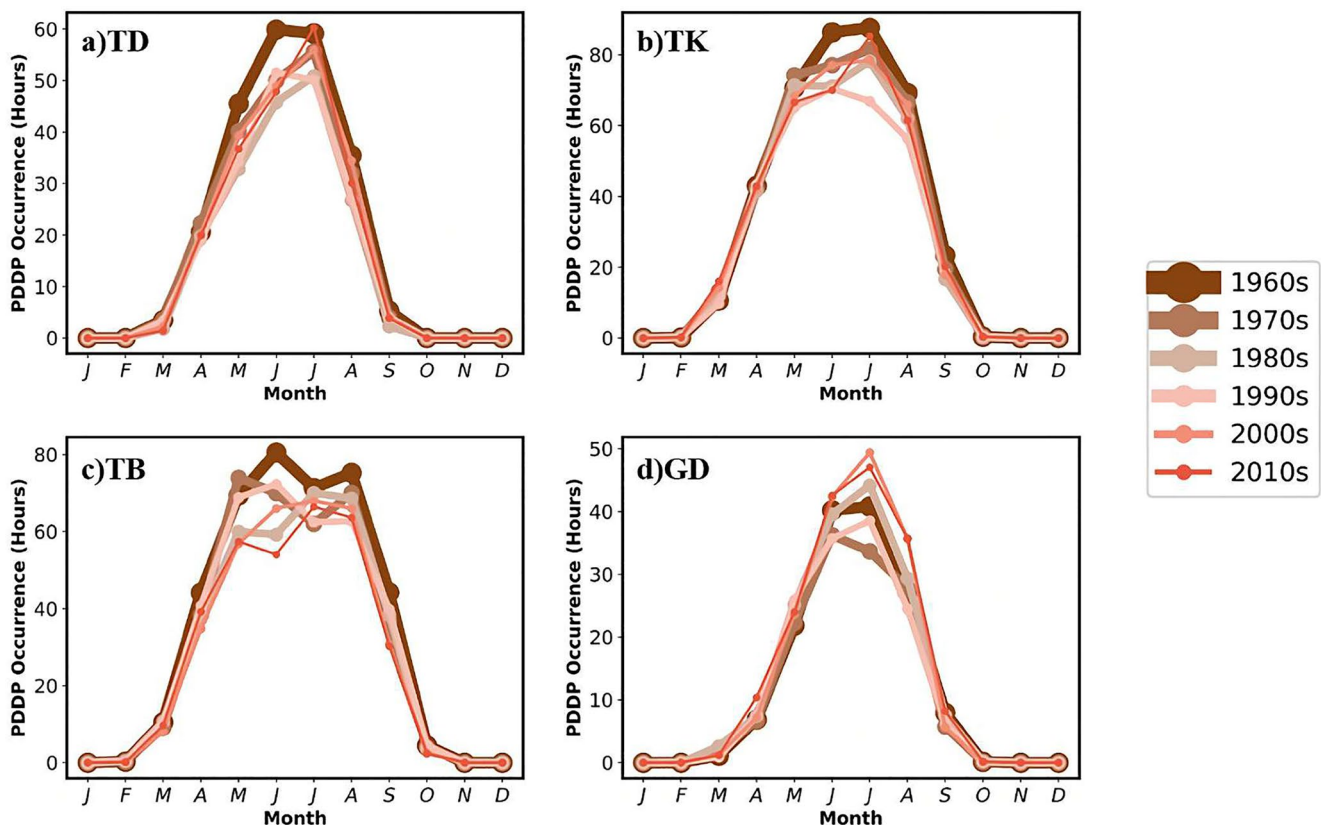


**Figure 7.** Monthly variation of potential dust devil and dusty plume at four study sites over the past decades calculated using ERA5 reanalysis data set.

no PDDP occurring after September. Unlike Figure 5, in different places, the peak position and the width of the curve varied greatly. The curves of the TD, TK, and GD were all single-peak structures, while the TB had a double-peak structure for some decades. The double-peak structure in TB was probably due to the uneven distribution of summer precipitation. The average precipitation from May to August was 20.11, 31.17, 37.02, and 27.21 mm, respectively, with standard deviation of over 7 mm. In the 2010s, the average precipitation from May to August was 22.11, 43.30, 38.13, and 31.65 mm, respectively, where the strong precipitation in June reduced the frequency of PDDP in June. While in the 1960s, the precipitation in 4 months was 21.25, 24.77, 33.89, and 23.56 mm, respectively, and the high precipitation in July caused the frequency of PDDP to decrease. Full width at half maximum (FWHM) that varies from region to region represents the time of the year when the frequency of PDDP is high, the larger the half-wave width, the longer the PDDP occurrence in a year. In the GD, FWHM occurred between May and August, while in the TB, it was between April and September, and for the TD and TK, FWHM was somewhere in between. For the peak shifts, there was a trend of peak movement from June to July in the GD and TD, and the peak in the TK area has been mostly in July except in the 1990s, while the peak position has been fluctuating in the TB area due to the influence of precipitation. The effect of volcanic eruptions on the frequency of dust devils is similar to that in Figure 6: Pinatubo eruption caused a significant decrease in the frequency of PDDP in the TD, TK, TB, and GD in the 1990s. Ma et al. (2020) presented the single-peaked distribution of monthly changes in dust emissions with a peak in July at the northern margin of the TD, while Han et al. (2016) gave the monthly changes of dust devil frequency in northwestern China with two peaks in March and June because the dust devil frequency in April was low due to strong winds.

Changes of PDDP during a day for the four regions calculated based on ERA5 are shown in Figure 8. The black line on the column is the error bar. All times in this chart have been converted to LT in accordance with the time zone divisions. PDDP primarily occurred in the middle of the day (10:00 LT–17:00 LT) with a peak at 13:00 LT and started occurring at different times in different regions. In deserts like the TD, GD, PDDP started to increase at 11:00 LT while in basin like the TK and TB, the frequency of PDDP was high from 10:00 LT onwards. PDDP frequency between 12:00 LT and 14:00 LT was more than 60% of the total frequency in the four regions, and for the TD, even reached 80%. Han et al. (2016) presented the diurnal changes in the frequency of dust devil which started at 9:00 LT, reached its maximum at 14:00 LT, and did not occur after 17:00 LT. While Sinclair (1966) found that diurnal changes of dust devil frequency followed a normal distribution with a peak in 13:00 LT–14:00 LT. All those previous studies showed a single peaked diurnal changes in dust devil frequency with a peak in 13:00LT–14:00LT which is consistent with our results.

### 3.3. Relationship Between Dust Devils and Meteorological Parameters

Under the context of global warming, interannual trends in the frequency of PDDP can vary considerably from region to region. These differences can be attributed to local meteorological factors, for example, precipitation, air temperature, and wind. This section studies how these factors influence PDDP occurrence.

The relationship between precipitation and PDDP frequency is given in Figure 9. Figure 9 contains a total of 252 points for 63 years in the four sites (TD, TK, TB, GD). The color of each point in Figure 9 maps the smoothed spatial density value (kernel density) at which the point is located that the darker the color of the dot, the higher the probability density of the dot. Anomaly rate on the vertical and horizontal coordinates is the value of that year minus the average of 63 years and divided by the average of 63 years. In this case, precipitation anomaly rate equals the precipitation of that year minus 63-year average divided 63-year average precipitation. While on the horizontal coordinate, PDDP frequency anomaly rate is equal to PDDP frequency of that year minus 63-year average divided by 63-year average PDDP frequency. Precipitation data is from ERA5 reanalysis data set by accumulating hourly data throughout the year while PDDP frequency is calculated using thermodynamic criteria given in Section 2.2. The frequency of PDDP and precipitation showed a significant negative correlation at the 99% confidence level. The increase in precipitation will reduce PDDP frequency, and the greater the increase in precipitation, the greater the reduction in PDDP occurrence. Under the context of global warming, the distribution of precipitation under different scenarios would be very different in 2100 compared to today (IPCC 6, 2021). Therefore, dust devil frequency might change significantly by then.

Figure 10 depicts the relationship between air temperature and PDDP frequency. Similar to Figure 9, it contains a total of 252 points for 63 years in four small regions (TD, TK, TB, GD), the darker the color of the dot, the higher the probability density of the dot. Anomaly rate is defined in the same way as in Figure 9, but the data are

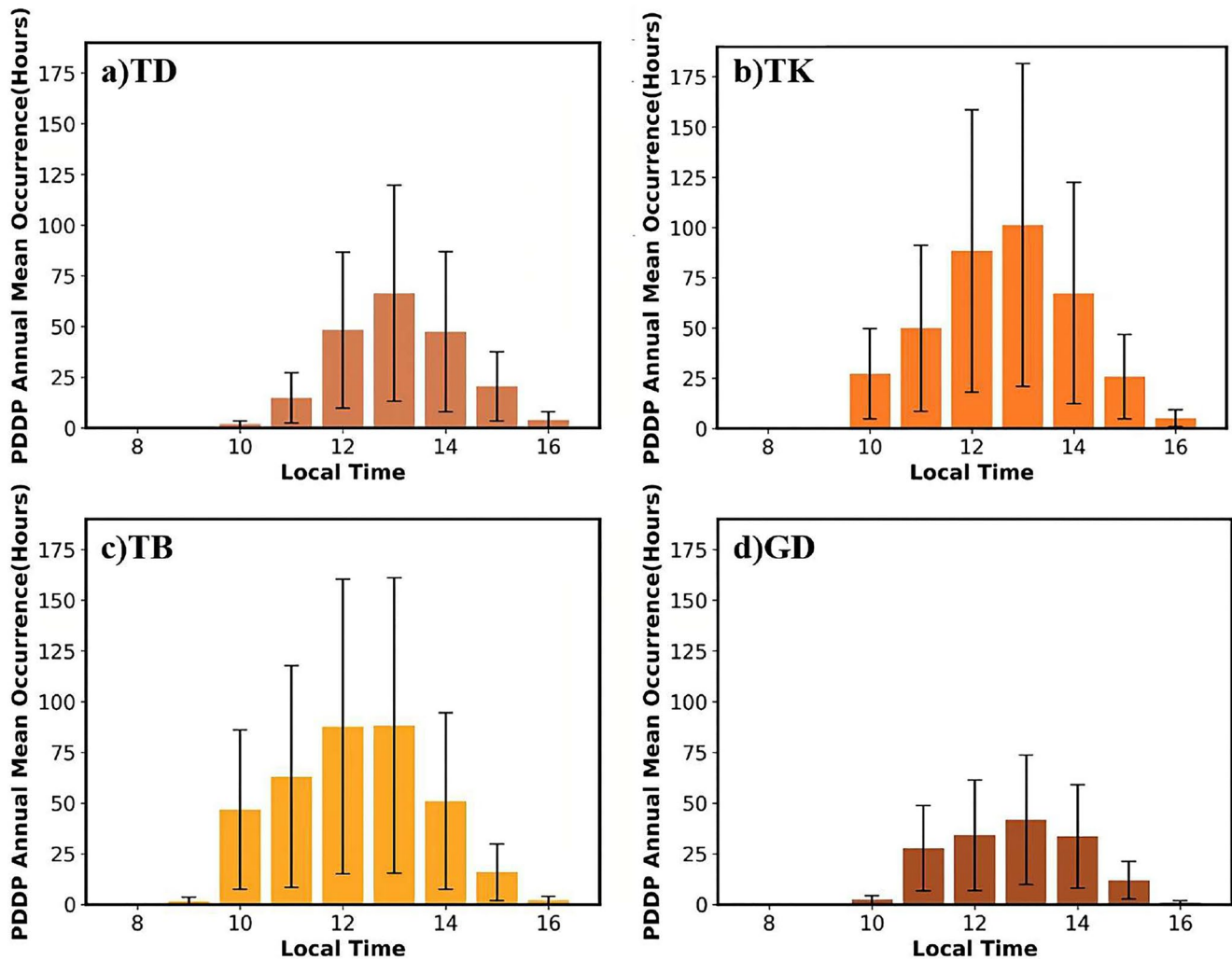


**Figure 8.** Diurnal variation of potential dust devil and dusty plume at four study regions in East Asia during 1959–2021 calculated using ERA5 reanalysis data set. Error bar represents standard deviation.

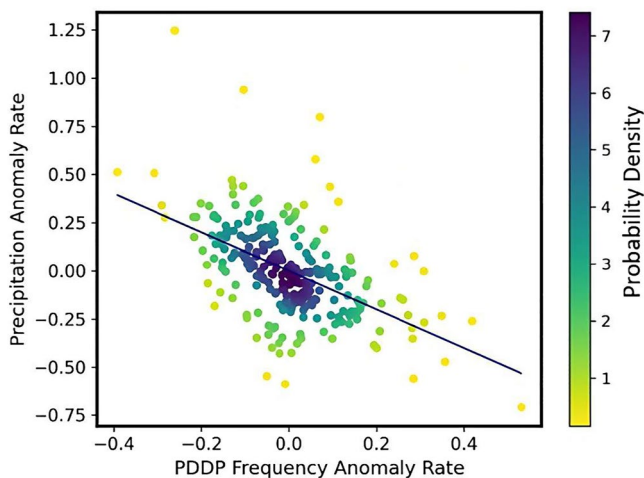


**Figure 9.** The relationship between precipitation and potential dust devil and dusty plume frequency in four study regions.

for June, July, and August, that is, summer rather than the whole year as the temperature fluctuated greatly during the year and PDDP mostly occurred at midday in summer. In order to clarify the relationship between the occurrence of PDDP and air temperature, the temperature data were averaged from 10:00 LT to 16:00 LT in accordance with Figure 9. Air temperature data are from ERA5 reanalysis data set at 2 m near the ground while PDDP frequency data is also in the corresponding time period. There is a significant positive correlation between air temperature and the frequency of PDDP ( $p < 0.01$ ), and the greater the increase in air temperature, the greater the frequency of dust devils. Compared to Figure 9, the effect of near-surface air temperature on dust devils is more diffuse than the effect of precipitation on dust devils. Under global warming, with the rise in temperature, the frequency of dust devils is likely to increase in the future. However, Sinclair (1966) discovered that the highest surface air temperature might not necessarily mean the highest dust devil frequency but the lowest atmospheric (vertical) stability might, implying that the frequency of dust devils could not be determined from the near-surface temperature alone. This is because the frequency of dust devils is influenced by many factors such as precipitation.

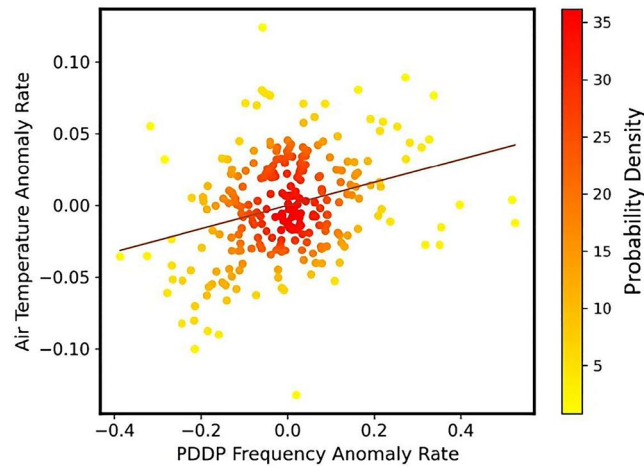


**Figure 10.** Same as Figure 9 but for air temperature.

The impact of wind speed on the frequency of PDDP is shown in Figure 11. The red bars represent the conditions at the time of the PDDP, while the blue bars represent the time throughout the day. The hourly wind data is from ERA5 reanalysis data set by the sum of 10 m u-component and 10 m v-component squared then averaged and only four sites (TD, TK, TB, GD) were counted. Figure 11 shows that the wind speed at the time of PDDP occurrence and throughout the day are both skewed with maximum in 2 m/s and 3 m/s, respectively. PDDP mainly occurred within the interval of wind speed 0–6 m/s. When the wind speed was greater than 8 m/s, PDDP basically ceased to happen. Oke et al. (2007) indicated the occurrence of dust devil at wind speed of around 1.5–7.5 m/s, while Ansmann et al. (2009) mentioned the favorable horizontal wind speed of 2–7 m/s. Han et al. (2016) has confirmed that strong winds are not conducive to the occurrence of dust devils. In that study, they found that dust devil frequency in April was lower than that in March due to frequent strong winds (>17 m/s) in April.

#### 4. Conclusions

This paper presented a detailed investigation of the long-term variation of PDDP in East Asia, and further analyzed the effect of different underlying surface and meteorological factors on PDDP, based on ERA5 reanalysis data set. The results show that weak PDDP accounted for about 68% of the total frequency, moderate intensity PDDP occurred about 27%, and strong PDDP happened less than 5% respectively. During 1959–2021, the PDDP frequency in East Asia generally exhibited a downward trend among which strong PDDP dropped significantly.

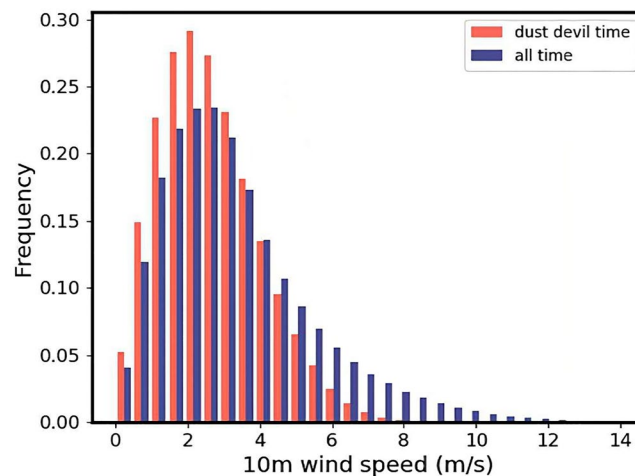


**Figure 11.** Frequency distribution of wind speed in the duration of potential dust devil and dusty plume and throughout the day.

Inter-annual trends in PDDP frequency also varied from region to region, with a significant increase in PDDP frequency in the Gobi Desert (GD) but a decrease in the Taklimakan Desert (TD). Moreover, PDDP in East Asia had a distinct seasonal distribution with the frequency of PDDP reaching the highest in summer. In addition, there was a peak for monthly variation of PDDP, shifting from June to July, over the past decades. Regarding the diurnal changes, PDDP mainly occurred between 10:00 LT and 16:00 LT, with over 60% of them occurring between 12:00 LT and 14:00 LT. Particularly, we found a negative correlation between precipitation and PDDP frequency. In addition, PDDP mainly occurred at wind speed of 0–6 m/s and almost no PDDP happened when the 10-m wind speed is larger than 8 m/s. This study provides a comprehensive understanding of PDDP in East Asia over the past decades, which is of great importance to further evaluate its impact on climate, environment as well as ecosystem.

### Data Availability Statement

The ERA5 reanalysis data set is available at <https://www.ecmwf.int/en/forecasts/dataset/ecmwf-reanalysis-v5> and can be downloaded using Climate Data Store (CDS) (Hersbach et al., 2018). Calculations and plotting have largely been performed using the Python software (Python Software Foundation, <https://www.python.org/>).

### Acknowledgments

This research was funded by the Second Tibetan Plateau Scientific Expedition and Research Program (STEP), Grant 2019QZKK0602; the Gansu Provincial Science and Technology Innovative Talent Program, the High-level Talent and Innovative Team Special Project (Chief Scientist System, No.22JR9KA001); Higher Education Discipline Innovation Project—111 Project (B 13045).

### References

- Allen, R. G., Pereira, L. S., Raes, D., & Smith, M. (1998). Crop evapotranspiration—Guidelines for computing crop water requirements. FAO Irrigation and drainage paper 56, Rome. Retrieved from <http://www.fao.org/docrep/X0490E/X0490E00.htm>
- Ansmann, A., Tesche, M., Knippertz, P., Bierwirth, E., Althausen, D., Müller, D., & Schulz, O. (2009). Vertical profiling of convective dust plumes in southern Morocco during SAMUM. *Tellus B*, 61(1), 340–353. <https://doi.org/10.1111/j.1600-0889.2008.00384.x>
- Balme, M., & Greeley, R. (2006). Dust devils on Earth and Mars. *Reviews of Geophysics*, 44(3). <https://doi.org/10.1029/2005RG000188>
- Carroll, J. J., & Ryan, J. A. (1970). Atmospheric vorticity and dust devil rotation. *Journal of Geophysical Research*, 75(27), 5179–5184. <https://doi.org/10.1029/JC075i027p05179>
- Deardorff, J. W. (1970). Convective velocity and temperature scales for the unstable planetary boundary layer and for Rayleigh convection. *Journal of the Atmospheric Sciences*, 27(8), 1211–1213. [https://doi.org/10.1175/1520-0469\(1970\)027<1211:CVATSF>2.0.CO;2](https://doi.org/10.1175/1520-0469(1970)027<1211:CVATSF>2.0.CO;2)
- Dee, D. P., Uppala, S. M., Simmons, A. J., Berrisford, P., Poli, P., Kobayashi, S., et al. (2011). The ERA-Interim reanalysis: Configuration and performance of the data assimilation system. *Quarterly Journal of the Royal Meteorological Society*, 137(656), 553–597. <https://doi.org/10.1002/qj.828>
- Després, V. R., Alex Huffman, J., Burrows, S. M., Hoose, C., Safatov, A. S., Buryak, G., et al. (2012). Primary biological aerosol particles in the atmosphere: A review. *Tellus Series B Chemical and Physical Meteorology*, 64(1), 15598. <https://doi.org/10.3402/tellusb.v64i0.15598>
- Dong, Q., Huang, Z., Li, W., Li, Z., Song, X., Liu, W., et al. (2022). Polarization lidar measurements of dust optical properties at the junction of the Taklimakan Desert–Tibetan Plateau. *Remote Sensing*, 14(3), 558. <https://doi.org/10.3390/rs14030558>
- Feng, S., & Fu, Q. (2013). Expansion of global drylands under a warming climate. *Atmospheric Chemistry and Physics*, 13(10), 081–094. <https://doi.org/10.5194/acp-13-10081-2013>
- Gao, C., Xiu, A., Zhang, X., Tong, Q., Zhao, H., Zhang, S., et al. (2022). Two-way coupled meteorology and air quality models in Asia: A systematic review and meta-analysis of impacts of aerosol feedbacks on meteorology and air quality. *Atmospheric Chemistry and Physics*, 22(8), 5265–5329. <https://doi.org/10.5194/acp-22-5265-2022>
- Gillette, D. A., & Sinclair, P. C. (1990). Estimation of suspension of alkaline material by dust devils in the United States. *Atmospheric Environment*, 24(5), 1135–1142. [https://doi.org/10.1016/0960-1686\(90\)90078-2](https://doi.org/10.1016/0960-1686(90)90078-2)
- Ginoux, P. M., Chin, I., Tegen, M., Prospero, B., Holben, O., Dubovik, O., & Lin, S. J. (2001). Sources and distributions of dust aerosols simulated with the GOCART model. *Journal of Geophysical Research*, 106(D17), 20255–20273. <https://doi.org/10.1029/2000JD000053>
- Gorelick, N., Hancher, M., Dixon, M., Ilyushchenko, S., Thau, D., & Moore, R. (2017). Google Earth Engine: Planetary-scale geospatial analysis for everyone. *Remote Sensing of Environment*, 202, 18–27. <https://doi.org/10.1016/j.rse.2017.06.031>
- Gu, Z. L., Qiu, J., Zhao, Y. Z., & Hou, X. P. (2008). Analysis on dust devil containing loess dusts of different sizes. *Aerosol & Air Quality Research*, 8(1), 65–77. <https://doi.org/10.4209/aaqr.2007.03.0026>
- Gu, Z. L., Wei, W., & Zhao, Y. Z. (2010). An overview of surface conditions in numerical simulations of dust devils and the consequent near-surface air flow fields. *Aerosol and Air Quality Research*, 10(3), 272–281. <https://doi.org/10.4209/aaqr.2009.12.0077>
- Han, Y., Wang, K., Liu, F., Zhao, T., Yin, Y., Duan, J., & Luan, Z. (2016). The contribution of dust devils and dusty plumes to the aerosol budget in western China. *Atmospheric Environment*, 126, 21–27. <https://doi.org/10.1016/j.atmosenv.2015.11.025>
- Hersbach, H., Bell, B., Berrisford, P., Biavati, G., Horányi, A., Muñoz Sabater, J., et al. (2018). ERA5 hourly data on single levels from 1959 to present. Copernicus Climate Change Service (C3S), Climate Data Store (CDS). <https://doi.org/10.24381/cds.adbb2d47>
- Hess, G. D., & Spillane, K. T. (1990). Characteristics of dust devils in Australia. *Journal of Applied Meteorology and Climatology*, 29(6), 498–507. [https://doi.org/10.1175/1520-0450\(1990\)029<0498:CODDIA>2.0.CO;2](https://doi.org/10.1175/1520-0450(1990)029<0498:CODDIA>2.0.CO;2)
- Huang, J., Wang, T., Wang, W., Li, Z., & Yan, H. (2014). Climate effects of dust aerosols over East Asian arid and semiarid regions. *Journal of Geophysical Research: Atmospheres*, 119(19), 11398–11416. <https://doi.org/10.1002/2014JD021796>
- Huang, J., Yu, H., Dai, A., Wei, Y., & Kang, L. (2017). Drylands face potential threat under 2°C global warming target. *Nature Climate Change*, 7(6), 417–422. <https://doi.org/10.1038/nclimate3275>
- Huang, J., Zhang, G., Zhang, Y., Guan, X., Wei, Y., & Guo, R. (2020). Global desertification vulnerability to climate change and human activities. *Land Degradation & Development*, 31(11), 1380–1391. <https://doi.org/10.1002/ldr.3556>
- Huang, Z., Huang, J., Bi, J., Wang, G., Wang, W., Fu, Q., et al. (2010). Dust aerosol vertical structure measurements using three MPL lidars during 2008 China–U.S. joint dust field experiment. *Journal of Geophysical Research*, 115, D00K15. <https://doi.org/10.1029/2009JD013273>

- Huang, Z., Nee, J. B., Chiang, C. W., Zhang, S., Jin, H., Wang, W., & Zhou, T. (2018). Real-time observations of dust–cloud interactions based on polarization and Raman lidar measurements. *Remote Sensing*, *10*(7), 1017. <https://doi.org/10.3390/rs10071017>
- Huang, Z., Wang, Y., Bi, J., Wang, T., Li, W., Li, Z., & Zhou, T. (2022). An overview of aerosol lidar: Progress and prospect. *National Remote Sensing Bulletin*, *26*(5), 834–851. <https://doi.org/10.11834/jrs.20221388>
- IPCC. (2021). *Climate change 2021: The physical science basis. contribution of Working Group I to the sixth assessment report of the Intergovernmental Panel on Climate Change* [V. Masson-Delmotte, P. Zhai, A. Pirani, S.L. Connors, C. Péan, S. Berger, N. Caud, Y. Chen, L. Goldfarb, M.I. Gomis, M. Huang, K. Leitzell, E. Lonnoy, J.B.R. Matthews, T.K. Maycock, T. Waterfield, O. Yelekçi, R. Yu, and B. Zhou (eds.)]. Cambridge University Press. <https://doi.org/10.1017/9781009157896>
- Jemmett-smith, B., Marsham, J., Knippertz, P., & Gilkeson, C. (2015). Quantifying global dust devil occurrence from meteorological analyses. *Geophysical Research Letters*, *42*(4), 1275–1282. <https://doi.org/10.1002/2015GL063078>
- Klose, M. (2014). Convective Turbulent Dust Emission: Process, parameterization, and relevance in the Earth system. (Doctoral dissertation, Universität zu Köln, urn:nbn:de:hbz:38-58264).
- Klose, M., Jemmett-Smith, B. C., Kahnp, H., Kahre, M., Knippertz, P., Lemmon, M. T., et al. (2016). Dust devil sediment transport: From lab to field to global impact. *Space Science Reviews*, 1–50. <https://doi.org/10.1007/s11214-016-0261-4>
- Klose, M., & Shao, Y. (2016). A numerical study on dust devils with implications to global dust budget estimates. *Aeolian Research*, *22*, 47–58. <https://doi.org/10.1016/j.aeolia.2016.05.003>
- Koch, J., & Renno, N. O. (2005). The role of convective plumes and vortices on the global aerosol budget. *Geophysical Research Letters*, *32*(18). <https://doi.org/10.1029/2005GL023420>
- Kok, J. F., Adebiyi, A. A., Albani, S., Balkanski, Y., Wan, J. S., Chin, M., et al. (2021). Contribution of the world's main dust source regions to the global cycle of desert dust. *Atmospheric Chemistry and Physics*, *21*(10), 8169–8193. <https://doi.org/10.5194/acp-21-8169-2021>
- Liu, C., Zhao, T., Yang, X., Liu, F., Han, Y., Luan, Z., et al. (2016). Observational study of formation mechanism, vertical structure, and dust emission of dust devils over the Taklimakan desert, China. *Journal of Geophysical Research: Atmospheres*, *121*(7), 3608–3618. <https://doi.org/10.1002/2015JD024256>
- Liu, J., Xin, Z., Huang, Y., & Yu, J. (2022). Climate suitability assessment on the Qinghai-Tibet Plateau. *Science of The Total Environment*, *816*, 151653. <https://doi.org/10.1016/j.scitotenv.2021.151653>
- Lyons, T. J., Nair, U. S., & Foster, I. J. (2008). Clearing enhances dust devil formation. *Journal of Arid Environments*, *72*(10), 1918–1928. <https://doi.org/10.1016/j.jaridenv.2008.05.009>
- Ma, M., Yang, X., Zhou, C., He, Q., & Mamtimin, A. (2020). Contributions of dusty weather and dust devil to dust emission amounts at the northern margin of the Taklimakan desert. *Natural Hazards*, *103*(1), 1441–1454. <https://doi.org/10.1007/s11069-020-04043-3>
- Mason, J. P., Patel, M. R., & Lewis, S. R. (2014). The retrieval of optical properties from terrestrial dust devil vortices. *Icarus*, *231*(4), 385–393. <https://doi.org/10.1016/j.icarus.2013.12.013>
- Oke, A., Tapper, N. J., & Dunkerley, D. (2007). Willy-willies in the Australian landscape: The role of key meteorological variables and surface conditions in defining frequency and spatial characteristics. *Journal of Arid Environments*, *71*(2), 201–215. <https://doi.org/10.1016/j.jaridenv.2007.03.008>
- Renno, N. O., Abreu, V. J., Koch, J., Smith, P. H., Hartogensis, O. K., De Bruin, H. A., et al. (2004). MATADOR 2002: A pilot field experiment on convective plumes and dust devils. *Journal of Geophysical Research*, *109*(E7), E07001. <https://doi.org/10.1029/2003JE002219>
- Ryan, J. A. (1972). Relation of dust devil frequency and diameter to atmospheric temperature. *Geophysical Research Letters*, *77*(36), 7133–7137. <https://doi.org/10.1029/JC077i036p07133>
- Self, S., Zhao, J.-X., Holasek, R. E., Torres, R. C., & King, A. J. (1993). The atmospheric impact of the 1991 Mount Pinatubo eruption. In *Fire and mud: Eruptions and lahars of Mount Pinatubo, Philippines*, No. NASA/CR-93-207274. University of Washington Press.
- Shao, Y., Wyrwoll, K., Chappell, A., Huang, J., Lin, Z., McTainsh, G. H., et al. (2011). Dust cycle: An emerging core theme in earth system science. *Aeolian Research*, *2*(4), 181–204. <https://doi.org/10.1016/j.aeolia.2011.02.001>
- Sinclair, P. C. (1966). *A quantitative analysis of the dust devil*. (PhD thesis). Univ. of Ariz. Retrieved from <http://hdl.handle.net/10150/565138>
- Sinclair, P. C. (1973). The lower structure of dust devils. *Journal of the Atmospheric Sciences*, *30*(8), 1599–1619. [https://doi.org/10.1175/1520-0469\(1973\)030<1599:TLSODD>2.0.CO;2](https://doi.org/10.1175/1520-0469(1973)030<1599:TLSODD>2.0.CO;2)
- Stull, R. B. (1988). *An introduction to boundary layer meteorology* (Vol. 13). Springer Science & Business Media. ISBN: 978-90-277-2769-5.
- Tang, Y., Han, Y., & Liu, Z. (2018). Temporal and spatial characteristics of dust devils and their contribution to the aerosol budget in East Asia—An analysis using a new parameterization scheme for dust devils. *Atmospheric Environment*, *182*, 225–233. <https://doi.org/10.1016/j.atmosenv.2018.03.050>
- Wang, J., Guan, X., Guan, Y., Zhu, K., Shi, R., Kong, X., & Guo, S. (2021). Changes in lengths of the four seasons over the drylands in the northern hemisphere midlatitudes. *Journal of Climate*, *34*(20), 8181–8190. <https://doi.org/10.1175/JCLI-D-20-0774.1>
- Zhang, S., Huang, Z., Li, M., Shen, X., Wang, Y., Dong, Q., et al. (2022). Vertical Structure of dust aerosols observed by a ground-based Raman lidar with polarization capabilities in the center of the Taklimakan desert. *Remote Sensing*, *14*(10), 2461. <https://doi.org/10.3390/rs14102461>
- Zhao, Y. Z., Gu, Z. L., Yu, Y. Z., Ge, Y., Li, Y., & Feng, X. (2004). Mechanism and large eddy simulation of dust devils. *Atmosphere-Ocean*, *42*(1), 61–84. <https://doi.org/10.3137/ao.420105>